

# Three-dimensional Icosahedral Phase Field Quasicrystal

P. Subramanian<sup>1</sup>, A.J. Archer<sup>2</sup>, E. Knobloch<sup>3</sup> and A.M. Rucklidge,<sup>1</sup>

<sup>1</sup>*Department of Applied Mathematics, University of Leeds, Leeds LS2 9JT, UK*

<sup>2</sup>*Department of Mathematical Sciences, Loughborough University, Loughborough LE11 3TU, UK*

<sup>3</sup>*Department of Physics, University of California at Berkeley, Berkeley CA 94720, USA*

(Dated: August 25, 2016)

We investigate the formation and stability of icosahedral quasicrystalline structures using a dynamic phase field crystal model. Nonlinear interactions between density waves at two length scales stabilize three-dimensional quasicrystals. We determine the phase diagram and parameter values required for the quasicrystal to be the global minimum free energy state. We demonstrate that traits that promote the formation of two-dimensional quasicrystals are extant in three dimensions, and highlight the characteristics required for three-dimensional soft matter quasicrystal formation.

PACS numbers: 61.44.-n, 61.44 Br, 81.10.Aj

Periodic crystals form ordered arrangements of atoms or molecules with rotation and translation symmetries, and possess discrete X-ray diffraction patterns, or equivalently, discrete spatial Fourier spectra. In contrast, quasicrystals (QCs) lack the translational symmetries of periodic crystals, yet also display discrete spatial Fourier spectra. QCs made from metal alloys were discovered in 1982 [1] and attracted the Nobel prize for chemistry in 2011. QCs can be quasiperiodic in all three dimensions (e.g., with icosahedral symmetry), or can be quasiperiodic in two (or one) directions while being periodic in one (or two). The vast majority of the QCs discovered so far are metallic alloys (e.g., Al/Mn or Cd/Ca). However, QCs have recently been found in nanoparticles [2], mesoporous silica [3], and soft matter [4] systems. The latter include micellar melts [5, 6] formed, e.g., from linear, dendrimer or star block copolymers. Recently, three-dimensional (3D) icosahedral QCs have been found in molecular dynamics simulations of particles interacting via a three-well pair potential [7].

In recent years, model systems in two dimensions (2D) have been studied in order to understand soft matter QC formation and stability [8–12]. Phase field crystal models have been employed to simulate the growth of 2D QCs [13] and the adsorption properties on a quasicrystalline substrate [14]. The ingredients for 2D quasipattern formation are, firstly, a propensity towards periodic density modulations with two characteristic wave numbers  $k_1$  and  $k_2$  [15–18]. The ratio  $k_2/k_1$  must be close to certain special values, e.g., for dodecagonal QCs the value is  $2 \cos \frac{\pi}{12}$ . Secondly, strong reinforcing (i.e., resonant) nonlinear interactions between these two characteristic density waves are required [17, 19, 20]. Earlier work on quasipatterns observed in Faraday wave experiments reveals similar requirements [19, 21–23]. We demonstrate here, following Mermin and Troian [24], that these same requirements suffice to stabilize icosahedral QCs in 3D. In contrast, nonlinear resonant interactions between density waves at a single wavelength are important in stabilizing simple crystal structures, such as body-centered

cubic (bcc) crystals [25] although, with the right coupling, QCs can also be stabilized [26].

We consider a 3D phase field crystal (PFC) model, appropriate for soft matter systems, that generates modulations with two length scales. The PFC model predicts the density distribution of the matter forming a solid or a liquid on the microscopic length scale of the constituent atoms or molecules, and takes the form of a theory for a dimensionless scalar field  $U(\mathbf{x}, t)$  that specifies the density deviation from its average value at position  $\mathbf{x}$  at time  $t$  [27]. This model consists of a nonlinear partial differential equation (PDE) with conserved dynamics, describing the time evolution of  $U$  over diffusive time scales [27]. Our PFC model includes all the resonant interactions that occur in the case of icosahedral symmetry. This not only extends previous work to three dimensions, but also allows for independent control over the growth rates of waves with the two wavelengths, and shows that, just as for 2D QCs, resonant interactions between the two wavelengths do stabilize 3D QCs.

Our PFC model starts with a free energy  $\mathcal{F}$ :

$$\mathcal{F}[U] = \int \left[ -\frac{1}{2}U\mathcal{L}U - \frac{Q}{3}U^3 + \frac{1}{4}U^4 \right] d\mathbf{x}, \quad (1)$$

where the operator  $\mathcal{L}$  and parameter  $Q$  are defined below. The evolution equation for  $U$  follows conserved dynamics and can be obtained from the free energy as

$$\frac{\partial U}{\partial t} = \nabla^2 \left( \frac{\delta \mathcal{F}[U]}{\delta U} \right) = -\nabla^2 (\mathcal{L}U + QU^2 - U^3). \quad (2)$$

This evolution equation describes a linearly unstable system that is stabilized nonlinearly by the cubic term. The relative importance of second order resonant interactions can be varied by setting the value of  $Q$ . The average value of  $U$  is conserved, so  $\bar{U}$  is effectively a parameter of the system. Without loss of generality we choose  $\bar{U} = 0$ , since other values can be accommodated by altering  $\mathcal{L}$  and  $Q$ .

The model is based on the original PFC model of Elder et al. [28], which allowed linear instability at a single length scale, stabilised by a cubic term. Subsequently,

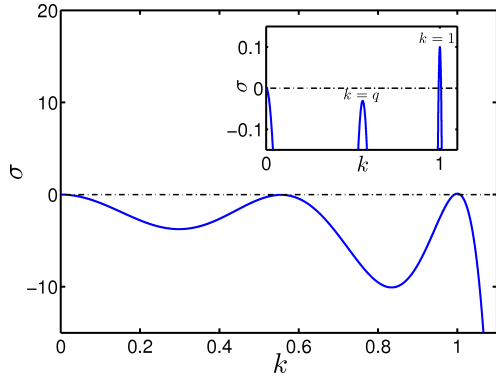


FIG. 1: Growth rate  $\sigma(k)$  as a function of the wave number  $k$  for the linear operator  $\mathcal{L}$  in Eq. (2), as defined in Eq. (3), with parameters  $\sigma_0 = -100$ ,  $q = 1/\tau \approx 0.6180$ ,  $\mu = 0.1$  and  $\nu = -0.1$ . The growth rates at  $k = 1$  and  $k = q$  are  $\mu$  and  $q^2\nu$ , as in the inset.

Achim et al. [13] used ideas based on the Lifshitz–Petrich model [19] to extend the problem to include two length scales. However, the growth rates of the two length scales in their models were constrained to be in a fixed ratio. In our model, we choose the linear operator  $\mathcal{L}$  (based on the one introduced by Rucklidge et al. [20]) to allow marginal instability at two wave numbers  $k = 1$  and  $k = q$ , with the growth rates of the two length scales determined by two independent parameters  $\mu$  and  $\nu$ , respectively. The resulting growth rate  $\sigma(k)$  of a mode with wave number  $k$  is given by a tenth-order polynomial:

$$\sigma(k) = \frac{k^4[\mu A(k) + \nu B(k)]}{q^4(1 - q^2)^3} + \frac{\sigma_0 k^2}{q^4}(1 - k^2)^2 (q^2 - k^2)^2, \quad (3)$$

where  $A(k) = [k^2(q^2 - 3) - 2q^2 + 4](q^2 - k^2)^2 q^4$  and  $B(k) = [k^2(3q^2 - 1) + 2q^2 - 4q^4](1 - k^2)^2$ . Figure 1 shows a typical  $\sigma(k)$ , with  $k = 0$  neutrally stable and  $k = q, 1$  weakly stable and unstable, respectively. The operator  $\mathcal{L}$  is obtained from Eq. (3) by first dividing by  $k^2$  and then replacing  $k^2$  by  $-\nabla^2$ .

The PFC model defined in Eq. (2) can be used to explore the effect of resonant triadic interactions on the resulting final structure. We encourage structures with icosahedral symmetry by setting the value of the wave number ratio  $q = 1/\tau$ , where  $\tau \equiv 2 \cos \frac{\pi}{5} \approx 1.6180$  is the golden ratio. The other parameters are  $\sigma_0$ ,  $\mu$ ,  $\nu$  and  $Q$ . In the rest of this paper, we set  $\sigma_0 = -100$  to ensure that the maxima in growth rate are sharp, and  $Q = 1$ , a value that is large enough for effective nonlinear interactions while still being amenable to weakly nonlinear analysis. We analyze the system in the remaining 2-parameter space, varying  $\mu$  and  $\nu$  simultaneously.

Three-dimensional direct numerical simulations of the PDE (2) were carried out in a periodic cubic domain of side length  $16 \times 2\pi$ , corresponding to 16 of the shorter of the two wavelengths. This choice is guided by the fact that domains that are twice a Fibonacci number (in this

case 8) allow our periodic solutions to approximate true QCs well. We used 192 Fourier modes (using FFTW [29]) in each direction and employed second-order exponential time differencing (ETD2) [30]. Simulations were carried out for 32 combinations of  $\mu$  and  $\nu$  lying on a circle of radius 0.1 in angular steps of  $\Delta\theta = 11.25^\circ$ . The simulations were started from an initial condition consisting of smoothed random values with an amplitude of  $\mathcal{O}(10^{-3})$  for each Fourier mode, and evolved to an asymptotic state. In cases where the solution did not decay to the zero flat state (corresponding to the uniform liquid), qualitatively distinct asymptotic states were found. These include hexagonal columnar crystals (hex), body-centered cubic crystals (bcc) at each of the two wavelengths, in addition to a 3D icosahedral QC. Examples of  $q$ -hex, 1-bcc and the icosahedral QC are shown in Figs. 2(a)–(c). Figure 2(d) shows a diffraction pattern with 5-fold symmetry for the QC. The peaks of this pattern do not lie precisely on the circles of radius 1 and  $q$  because the chosen periodic domain size only allows for an approximation to the irrational number  $q = 1/\tau$ . This discrepancy decreases with larger domain sizes, thus improving the resolution of the diffraction pattern, as shown in [31].

The stability of QCs is promoted by nonlinear wave interactions between three or more waves. In Ref. [26], it is pointed out that density perturbation waves (at one length scale) of the form  $e^{i\mathbf{k}\cdot\mathbf{x}}$  with wavevectors chosen to be the 30 edge vectors of an icosahedron can take advantage of three-wave interactions (from the triangular faces) and of five-wave interactions (from the pentagons surrounding five triangular faces, see Fig. 3(a)) to lower the free energy and so encourage the formation of icosahedral QCs. This results in having density waves involving 30 wavevectors, see Fig. 3 and Table I.

With two length scales in the golden ratio  $\tau$ , an alternative mechanism for reinforcing icosahedral symmetry is possible using only three-wave interactions. Taking five edge vectors of a pentagon adding up to zero, for example,  $\mathbf{k}_{16} + \mathbf{k}_7 + \mathbf{k}_{15} + \mathbf{k}_2 + \mathbf{k}_{25} = 0$  (see Table I), we use the fact that  $\mathbf{k}_7 + \mathbf{k}_{15} = \mathbf{q}_2$  and  $\mathbf{k}_2 + \mathbf{k}_{25} = \mathbf{q}_4$  to identify a three-wave interaction between  $\mathbf{q}_2$ ,  $\mathbf{q}_4$  and  $\mathbf{k}_{16}$  since these sum to zero. Many other three-wave interactions are possible.

We can now analyse the QCs of the type shown in Fig. 2(c). At small amplitudes,  $U$  can be rescaled in terms of a small parameter  $\epsilon$  as  $U = \epsilon U_1$ . Substituting this into the expression for the free energy and requiring that the three terms contribute at the same order implies the scaling  $Q = \epsilon Q_1$  and  $\mathcal{L}U = \mathcal{O}(\epsilon^3)$ . The scaling of the linear operator can be arranged by requiring that  $U_1$  is a combination of Fourier modes with wave numbers  $k = 1$  and  $k = q$  and that the parameters  $\mu$  and  $\nu$ , which govern the linear growth rates of these two wave numbers, scale as  $\mathcal{O}(\epsilon^2)$ . Upon substituting these expressions into Eq. (2), we observe that the time evolution occurs on a

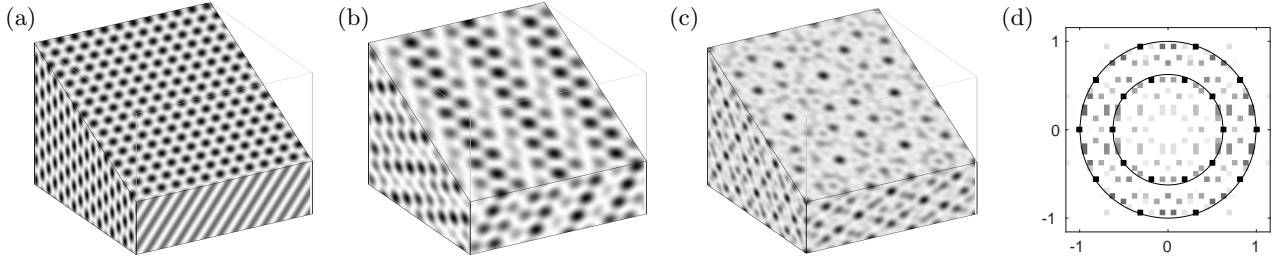


FIG. 2: (a) Hexagonal columnar phase with wave number  $q$  ( $q$ -hex) at  $(\mu, \nu) = (0.082, 0.056)$ . (b) Body centered cubic crystal with wave number 1 (1-bcc) at  $(\mu, \nu) = (-0.1, 0)$ . (c) Icosahedral quasicrystal (QC) at  $(\mu, \nu) = (-0.071, -0.071)$ . Each box has had a slice cut away, chosen to reveal the 5-fold rotation symmetry in (c). See [31] for more details on the quasicrystalline structure. (d) Diffraction pattern taken in a plane normal to the vector  $(\tau, -1, 0)$  in Fourier space. The circles of radii 1 and  $q$  are indicated. The 5-fold rotation symmetry of the diffraction pattern is indicated by the 10 peaks observed on each circle.

slow time scale, of order  $\mathcal{O}(\epsilon^{-2})$ .

For icosahedral QCs, we use the vectors from Table I and expand  $U_1$  as

$$U_1 = \sum_{j=1}^{15} z_j e^{i\mathbf{k}_j \cdot \mathbf{x}} + \sum_{j=1}^{15} w_j e^{i\mathbf{q}_j \cdot \mathbf{x}} + c.c., \quad (4)$$

where  $c.c.$  refers to the complex conjugate. The amplitudes  $z_j$  and  $w_j$  are functions of time and describe the evolution of modes with wave numbers 1 and  $q$ .

Substituting this expression for  $U_1$  into Eq. (1), we can write the rescaled volume-specific free energy  $f = \mathcal{F}/(V\epsilon^4)$  as

$$\begin{aligned} f = & -\mu z_1 \bar{z}_1 - 4Q(w_{10}z_4 - w_{11}z_5 - w_{12}z_2 - w_{13}z_3 \\ & - w_3w_5 - w_2w_4 - z_6z_8 - z_7z_9)\bar{z}_1 \\ & - \mu \sum_{j=2}^{15} |z_j|^2 - \nu \sum_{j=1}^{15} |w_j|^2 \\ & - Q(152 \text{ other cubic terms}) \\ & - (1305 \text{ quartic terms}), \end{aligned} \quad (5)$$

where we have written the contributions involving  $\bar{z}_1$  explicitly up to cubic order. All other contributions are of similar structure. Nonlinear terms at every order  $n$  contain combinations of  $n$  vectors that sum to zero. The evolution on the slow time scale of the amplitudes of the

$j$	$\mathbf{k}_j$	$j$	$\mathbf{k}_j$	$j$	$\mathbf{k}_j$
1	(1, 0, 0)	6	$\frac{1}{2}(1, \tau - 1, \tau)$	11	$\frac{1}{2}(\tau - 1, \tau, -1)$
2	$\frac{1}{2}(\tau, 1, \tau - 1)$	7	$\frac{1}{2}(1, \tau - 1, -\tau)$	12	$\frac{1}{2}(\tau - 1, -\tau, -1)$
3	$\frac{1}{2}(\tau, 1, 1 - \tau)$	8	$\frac{1}{2}(1, 1 - \tau, -\tau)$	13	$\frac{1}{2}(\tau - 1, -\tau, 1)$
4	$\frac{1}{2}(\tau, -1, 1 - \tau)$	9	$\frac{1}{2}(1, 1 - \tau, \tau)$	14	(0, 1, 0)
5	$\frac{1}{2}(\tau, -1, \tau - 1)$	10	$\frac{1}{2}(\tau - 1, \tau, 1)$	15	(0, 0, 1)

TABLE I: Indexed table of edge vectors  $\mathbf{k}_1, \dots, \mathbf{k}_{15}$  of an icosahedron with edges of length 1, following Ref. [32]. The remaining 15 are the negatives:  $\mathbf{k}_{j+15} = -\mathbf{k}_j$ . The 30 vectors on the other sphere, of radius  $q = 1\tau$ , are obtained by setting  $\mathbf{q}_j = \mathbf{k}_j/\tau$ ,  $j = 1, \dots, 30$ .

components of  $U_1$  is thus governed by the equations

$$\dot{z}_j = -\frac{\partial f}{\partial \bar{z}_j} \quad \text{and} \quad \dot{w}_j = -q^2 \frac{\partial f}{\partial \bar{w}_j}. \quad (6)$$

These evolution equations are the projection of the PDE (2) onto the 60 Fourier modes.

It is straightforward to find subsets of non-zero amplitudes that give equilibrium solutions that describe simple structures, such as lamellae (lam), hexagonal (hex) columnar crystals, and simple cubic crystals, at each length scale. More complex structures typically involve both length scales; these include 2D planar QCs (possibly periodic in the third direction), 3D columnar rhombic crystals, 3D orthorhombic crystals and 3D QCs with icosahedral or 5-fold symmetry. Within each class of solutions, we write down amplitude equations restricted to that class and solve the resulting coupled algebraic equations to obtain equilibrium solutions using the Bertini numerical algebraic geometry software package [33]. Using expression (5), we calculate the minimum free energy  $f$  associated with each class of solutions. By minimizing this over all classes of solutions at a given combination of  $\mu$  and  $\nu$ , we calculate the globally stable solution. Since we found body-centered cubic (bcc) crystals in Fig. 2(b), and since these cannot be represented in terms of the icosahedral basis vectors, we compute their free energy as a separate calculation, choosing a different set of basis vectors [34].

Figure 4 shows regions in the  $(\mu, \nu)$  plane, identifying the globally stable solution in each region. Body-centered cubic and hexagonal columnar crystals are observed at both wavelengths independently, and their regions of global stability are symmetric with respect to the  $\mu = \nu$  line. This symmetry is a consequence of the particular structure of the model. At larger values of  $\mu$  and  $\nu$ , the regions of 1-hex and  $q$ -hex are bounded, likewise symmetrically, by lamellar patterns 1-lam and  $q$ -lam, above the lines  $\mu = 1.91$  and  $\nu = 1.91$ , respectively. In particular, if either  $\mu$  or  $\nu$  is strongly negative while the other is increased, we recover the standard transition from zero to bcc to columnar hexagons to lamellae found in an investigation of a single lengthscale 3D phase field crystal

model [35]. However, when the linear growth rates  $\mu$  and  $\nu$  are both negative but not too negative, the global energy minimum corresponds instead to three-dimensional QCs. The resulting QC region opens out as  $Q$  increases from zero. The region labeled ‘zero’ indicates that here the trivial state  $U = 0$  is globally stable.

The local (linear) stability of the equilibria is obtained by linearizing the amplitude equations (6). The regions of local stability extend beyond the lines demarcating the boundaries of the regions of global stability, and many locally stable structures can coexist at given parameter combinations.

Figure 5 shows the variation of the specific free energy  $f$  in Eq. (5) around the dashed circle shown in Fig. 4. We focus on negative free energies only (i.e., states with energy lower than the uniform density liquid state), and from the figure we can read off the parameter range where each structure emerges as the global minimum. In spite of the large number of three-wave interactions in the icosahedral structure, 3D QCs emerge as globally stable states only over a limited range of angles ( $213.53^\circ \leq \theta \leq 236.47^\circ$ ). In the range of parameters investigated here, 2D planar QCs, 3D columnar rhombic crystals, 3D orthorhombic crystals and axial quasicrystals [36] (not shown) are never globally stable.

Hollow circles in the inset in Fig. 5 show the free energies of locally stable quasicrystalline steady states of the PDE (2), started from an initial condition with the QC imprinted. The fact that the solid line for the quasicrystalline free energy (from the small  $\epsilon$  asymptotics) is close to the hollow circles (from the PDE), both with respect to the value of the free energy and the range of linear stability, supports the validity of the asymptotics, despite the mathematical subtleties associated with QCs, identified in [37], and partly resolved in [38].

The parameters  $Q$  and  $\sigma_0$  were chosen so as to allow good agreement between minima of the free energy (1) and its weakly nonlinear approximation derived in Eq. (5). This agreement, and the prediction from the asymptotics that the region where QCs are globally stable vanishes when  $Q = 0$ , confirms that the contribution

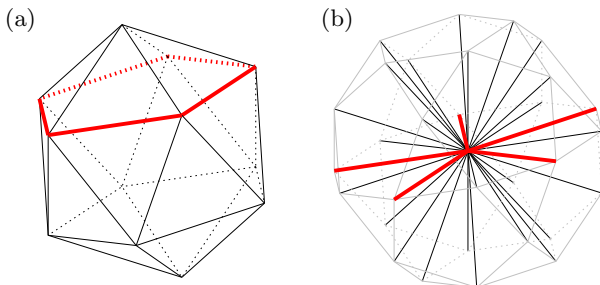


FIG. 3: (a) Icosahedron, with five edge vectors that add up to zero indicated with thick red lines (color online). (b) With the 30 edge vectors moved to the origin (the same five are indicated), the resulting figure is an icosidodecahedron.

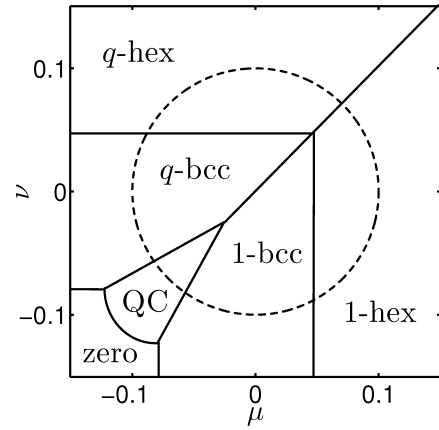


FIG. 4: Structures with minimal specific free energy  $f$  over a range of parameters  $\mu$  and  $\nu$ , computed as equilibria of the amplitude equations (6). PDE calculations are performed on the dashed circle around the origin with radius 0.1. The region in the third quadrant labeled ‘zero’ indicates that the trivial state  $U = 0$  is globally stable.

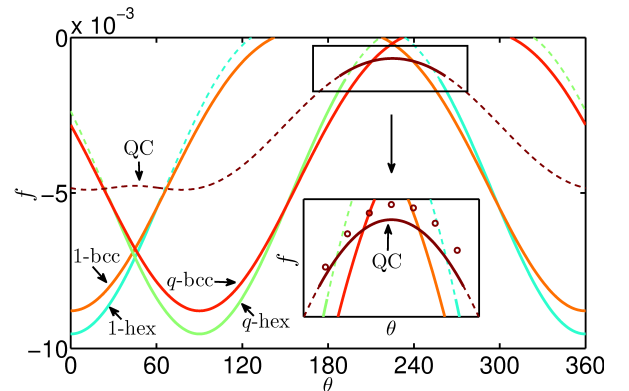


FIG. 5: (Color online) Variation of specific free energy  $f$  with angle  $\theta$  on a circle in the  $(\mu, \nu)$  plane of radius 0.1. Lines track the variation of free energy  $f$  of the labeled structures, solid where these are locally stable, dashed where they are locally unstable. We do not make this distinction for the bcc crystals as these use a different set of basis vectors and so their linear stability cannot be compared directly with that of QCs. The zero state,  $f = 0$ , corresponds to the uniform liquid. Hollow circles in the inset show the free energies of locally stable quasicrystalline asymptotic steady states from PDE calculations starting from an initial condition of the imprinted QC.

to the free energy from three-wave interactions is crucial in stabilizing 3D icosahedral QCs. The range of the linear growth rates  $(\mu, \nu)$  over which QCs are the global minimum of the free energy is relatively small, but expands when  $Q$  is larger or  $\sigma_0$  is less negative.

In conclusion, we have demonstrated that the nonlinear resonant mechanism that operates in 2D also stabilizes 3D icosahedral QCs as global minima of the free energy. This success will guide our future work in analyzing the formation of QCs in polymeric systems using realistic dynamical density functional theory, extending

the theory from [12] to three dimensions. Another avenue to explore lies in characterizing the symmetry subspaces that are retained in a QC structure using group-theoretic methods together with identifying the members of each symmetry subspace through a weakly nonlinear analysis.

We are grateful to Ron Lifshitz, Peter Olmsted, Daniel Read and Paul Matthews for many discussions, and to the anonymous referees for their constructive comments. This work was supported in part by the National Science Foundation under grant DMS-1211953 (EK).

- 
- [1] D. Shechtman, I. Blech, D. Gratias, and J. W. Cahn, *Phys. Rev. Lett.* **53**, 1951 (1984).
- [2] D. V. Talapin, E. V. Shevchenko, M. I. Bodnarchuk, X. Ye, J. Chen, and C. B. Murray, *Nature* **461**, 964 (2009).
- [3] C. Xiao, N. Fujita, K. Miyasaka, Y. Sakamoto, and O. Terasaki, *Nature* **487**, 349 (2012).
- [4] T. Dotera, *Israel J. Chem.* **51**, 1197 (2011).
- [5] X. Zeng, G. Ungar, Y. Liu, V. Percec, A. E. Dulcey, and J. K. Hobbs, *Nature* **428**, 157 (2004).
- [6] S. Fischer, A. Exner, K. Zielske, J. Perlich, S. Deloudi, W. Steurer, P. Lindner, and S. Förster, *Proc. Nat. Acad. Sci.* **108**, 1810 (2011).
- [7] M. Engel, P. F. Damasceno, C. L. Phillips, and S. C. Glotzer, *Nature Materials* **14**, 109 (2014).
- [8] K. Barkan, H. Diamant, and R. Lifshitz, *Phys. Rev. B* **83**, 172201 (2011).
- [9] A. J. Archer, A. M. Rucklidge, and E. Knobloch, *Phys. Rev. Lett.* **111**, 165501 (2013).
- [10] T. Dotera, T. Oshiro, and P. Ziherk, *Nature* **506**, 208 (2014).
- [11] K. Barkan, M. Engel, and R. Lifshitz, *Phys. Rev. Lett.* **113**, 098304 (2014).
- [12] A. J. Archer, A. M. Rucklidge, and E. Knobloch, *Phys. Rev. E* **92**, 012324 (2015).
- [13] C. V. Achim, M. Schmiedeberg, and H. Löwen, *Phys. Rev. Lett.* **112**, 255501 (2014).
- [14] J. Rottler, M. Greenwood, and B. Ziebarth, *J. Phys. Cond. Mat.* **24**, 135002 (2012).
- [15] W. S. Edwards, and S. Fauve, *Phys. Rev. E* **47**, R788 (1993).
- [16] H. W. Müller, *Phys. Rev. E* **49**, 1273–1277 (1994).
- [17] R. Lifshitz, and H. Diamant, *Phil. Mag.* **87**, 3021 (2007).
- [18] M. Engel and H.-R. Trebin, *Z. Kristallogr.* **223**, 721 (2008).
- [19] R. Lifshitz and D. M. Petrich, *Phys. Rev. Lett.* **79**, 1261 (1997).
- [20] A. M. Rucklidge, M. Silber, and A. C. Skeldon, *Phys. Rev. Lett.* **108**, 074504 (2012).
- [21] W. Zhang and J. Viñals, *J. Fluid Mech.* **336**, 301 (1997).
- [22] C. M. Topaz, J. Porter and M. Silber, *Phys. Rev. E* **70**, 066206 (2004).
- [23] A. M. Rucklidge and M. Silber, *SIAM J. Appl. Dyn. Sys.* **8**, 298 (2009).
- [24] N. D. Mermin and S. M. Troian, *Phys. Rev. Lett.* **54**, 1524 (1985).
- [25] S. Alexander and J. McTague, *Phys. Rev. Lett.* **41**, 702 (1978).
- [26] P. Bak, *Phys. Rev. Lett.* **54**, 1517 (1985).
- [27] H. Emmerich, H. Löwen, R. Wittkowski, T. Gruhn, G. I. Tóth, G. Tegze, and L. Gránásy, *Adv. Phys.* **61**, 665 (2012).
- [28] K. R. Elder, M. Katakowski, M. Haataja, and M. Grant, *Phys. Rev. Lett.* **88**, 245701 (2002).
- [29] M. Frigo and S. G. Johnson, *Proc. IEEE* **93**, 216 (2005).
- [30] S. M. Cox and P. C. Matthews, *J. Comp. Phys.* **176**, 430 (2002).
- [31] P. Subramanian, A. J. Archer, E. Knobloch, and A. M. Rucklidge, *Supplementary material for the paper Three-dimensional Icosahedral Phase Field Quasicrystal* (2016).
- [32] D. Levine and P. J. Steinhardt, *Phys. Rev. B* **34**, 596 (1986).
- [33] D. J. Bates, J. D. Hauenstein, A. J. Sommese, and C. W. Wampler, *Bertini: Software for Numerical Algebraic Geometry* (2013).
- [34] T. K. Callahan and E. Knobloch, *Nonlinearity* **10**, 1179 (1997).
- [35] A. Jaatinen and T. Ala-Nissila, *J. Phys. Cond. Mat.* **22**, 205402 (2010).
- [36] A. I. Goldman and R. F. Kelton, *Rev. Mod. Phys.* **65**, 213 (1993).
- [37] A. M. Rucklidge and W. J. Rucklidge, *Physica D: Nonlinear Phenomena* **178**, 62 (2003).
- [38] G. Iooss and A. M. Rucklidge, *J. Nonlin. Sci.* **20**, 361 (2010).